BIOCHEMISTRY
including biophysical chemistry & molecular biology

ARTICLE

pubs.acs.org/biochemistry

# Conformational Flexibility of a Human Immunoglobulin Light Chain Variable Domain by Relaxation Dispersion Nuclear Magnetic Resonance Spectroscopy: Implications for Protein Misfolding and Amyloid Assembly

Sujoy Mukherjee, Simon P. Pondaven, and Christopher P. Jaroniec*

Department of Chemistry, The Ohio State University, Columbus, Ohio 43210, United States

Supporting Information

**ABSTRACT:** The conformational flexibility of a human immunoglobulin κIV light-chain variable domain, LEN, which can undergo conversion to amyloid under destabilizing conditions, was investigated at physiological and acidic pH on a residue-specific basis by multidimensional solution-state nuclear magnetic resonance (NMR) methods. Measurements of backbone chemical shifts and amide $^{15}$N longitudinal and transverse spin relaxation rates and steady-state nuclear Overhauser enhancements indicate that, on the whole, LEN retains its native three-dimensional fold and dimeric state at pH 2 and that the protein backbone exhibits limited fast motions on the picosecond to nanosecond time scale. On the other hand, $^{15}$N Carr−Purcell−Meiboom−Gill (CPMG) relaxation dispersion NMR data show that LEN experiences considerable slower, millisecond time scale dynamics, confined primarily to three contiguous segments of about 5−20 residues and encompassing the N-terminal β-strand and complementarity determining loop regions 2 and 3 in the vicinity of the dimer interface. Quantitative analysis of the CPMG relaxation dispersion data reveals that at physiological pH these slow backbone motions are associated with relatively low excited-state protein conformer populations, in the ∼2−4% range. Upon acidification, the minor conformer populations increase significantly, to ∼10−15%, with most residues involved in stabilizing interactions across the dimer interface displaying increased flexibility. These findings provide molecular-level insights about partial protein unfolding at low pH and point to the LEN dimer dissociation, initiated by increased conformational flexibility in several well-defined regions, as being one of the important early events leading to amyloid assembly.

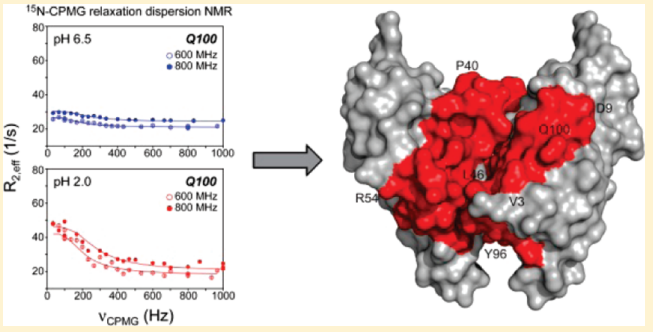


The process of conformational conversion of normally soluble proteins into large oligomeric aggregates and amyloid fibrils has been linked to over 40 human disease states.[1,2] The most widespread systemic disease of this type in the Western Hemisphere, light-chain amyloidosis (AL), is associated with the deposition in organs and tissues, including kidneys, lymphatic vessels, and heart, of amyloid fibrils composed of immunoglobulin (Ig) light-chain variable domains ($V_L$) of the λ or κ family.[3,4] It has previously been proposed that specific amino acid mutations to their germline sequences alter the thermodynamic stabilities of certain Ig $V_L$s, predisposing them toward aggregation and amyloid formation *in vivo*.[5−9] As suggested by comparative structural studies,[10−15] these processes are likely initiated by partial disruption of the native secondary, tertiary, and quaternary structure, a common motif encountered for numerous other amyloidogenic proteins,[1,2] though the nature of the partially unfolded conformers implicated in the earliest stages of aggregation is generally poorly understood on a residue-specific basis for immunoglobulin domains. This is primarily due to the fact that, with notable exceptions,[16] most biophysical techniques cannot readily probe at atomic level detail higher-energy, amyloidogenic protein states present at low concentration.

Here, we focus on a thorough investigation of the initial events leading to the misfolding and amyloid formation for LEN, a 114 amino acid (aa) human immunoglobulin κIV light-chain variable domain extracted as a Bence−Jones protein from a patient suffering from multiple myeloma.[17,18] In analogy to most other immunoglobulin domains of this type,[3,4] LEN is nonamyloidogenic *in vivo* and the recombinant form of the protein is a stable dimer under physiological conditions *in vitro*.[18] Conversely, under destabilizing conditions including both vigorous agitation and acidic pH[19−21] or the presence of denaturant molecules,[6,22] the protein can be induced to undergo conversion to the amyloid state. Thus,

**Received:** March 19, 2011
**Revised:** May 29, 2011
**Published:** May 31, 2011

LEN serves as a highly tractable model for exhaustive studies of the molecular basis of Ig $V_L$ aggregation, particularly in light of the fact that a closely related protein with high degree of sequence identity, dubbed SMA and differing from LEN at only eight aa positions (S29N, K30R, P40L, Q89H, T94H, Y96Q, S97T, and I106L), was the main component of amyloid deposits isolated from an AL patient[17,18] and found to aggregate readily *in vitro* at both physiological and low pH.[6,18,23] In a series of systematic studies, Fink and co-workers[19−21] have established that at pH ∼2 LEN retains a largely native-like character, with slight destabilization of the dimeric species likely serving as the initial trigger for protein aggregation. However, these studies, using a variety of biophysical methods of intrinsically low resolution, focused on the macroscopic nature of macromolecular structure and association and thus were not able to probe quantitatively and with residue-specific detail the changes in structural and dynamic characteristics of LEN upon acidification en route to amyloid formation.

Solution-state nuclear magnetic resonance (NMR) spectroscopy offers a unique set of tools for investigating the structure and motions of protein molecules over a wide range of time scales, from picoseconds to seconds,[24−26] with recent advances enabling studies of "invisible" protein excited states at populations as low as ∼0.5% of the major, ground-state conformer.[27−29] This methodology facilitates comprehensive analysis of protein unfolding phenomena frequently associated with aggregation and is highly complementary to other techniques traditionally used to probe amyloid formation and architecture, including hydrogen−deuterium exchange,[30−35] electron paramagnetic resonance,[36,37] and solid-state NMR.[38,39] In this work, we apply a suite of multidimensional solution-state NMR methods toward the quantitative, site-resolved analysis of the conformational flexibility of LEN on multiple time scales and use our findings to provide insights into the initial stages of low pH-induced protein misfolding and assembly into amyloid fibrils.

## EXPERIMENTAL PROCEDURES

**NMR Sample Preparation.** The LEN plasmid[18] was kindly provided by Dr. Fred J. Stevens (Argonne National Laboratory). $^{15}$N- and $^{13}$C,$^{15}$N-labeled proteins were overexpressed in *Escherichia coli* and purified as described previously.[40] Two samples were used for the NMR relaxation measurements, each consisting of $^{15}$N-labeled LEN at a concentration of 1.7 mM in aqueous solution with a total volume of ∼280 μL loaded into a Shigemi microcell. The first sample was prepared in pH 6.5 sodium phosphate buffer (20 mM sodium phosphate, 100 mM NaCl, 7% (v/v) $D_2O$ and 0.02% (w/v) $NaN_3$). The second sample contained ∼15 mM HCl, 100 mM NaCl, 7% $D_2O$, and 0.02% $NaN_3$ at pH 2.0. Two additional samples were utilized to establish the backbone resonance assignments of LEN at pH 2. One sample consisted of 1.5 mM $^{13}$C,$^{15}$N-LEN in the pH 2.0 HCl/NaCl solution in a Shigemi microcell, and the second sample contained 0.8 mM $^{15}$N-labeled LEN in the sodium phosphate buffer described above in a conventional 5 mm sample tube (Wilmad-Labglass, Buena, NJ); the latter sample was used to record a successive series of two-dimensional (2D) $^{15}$N−$^{1}$H heteronuclear single quantum coherence (HSQC) spectra at pH values of 7.4, 7.2, 6.9, 6.7, 6.5, 6.1, 5.2, 4.2, 3.1, 2.1, 2.9, 4.0, 5.0, 6.0, and 7.0 ± 0.1, with the pH adjusted by adding small amounts of concentrated HCl or NaOH and measured directly inside the NMR tube by using a specialized electrode (Hamilton, Reno, NV).

**NMR Spectroscopy.** NMR measurements were performed at 25 °C on Bruker DMX-600, DRX-600, and DRX-800 spectrometers equipped with either a room-temperature TXI probe with triple-axis gradients (DMX-600) or cryogenic probes with *z*-axis gradients (DRX-600 and DRX-800). All pulse schemes used were gradient and sensitivity enhanced[41,42] and employed water flip-back and 3−9−19 binomial pulses for optimum solvent suppression.[26] In addition, for all experiments that employed periods during which a variable amount of high-power radio-frequency (RF) irradiation was applied to the sample, a constant duty cycle was maintained by incorporating additional RF pulses following the free-induction decay (FID) acquisition to compensate for potential sample heating effects.[43]

Residue-specific backbone amide $^{15}$N longitudinal ($R_1$) and transverse ($R_2$) relaxation rates and steady-state heteronuclear $\{^{1}H\}-^{15}N$ nuclear Overhauser enhancements (NOEs), which report on protein motions on the picosecond (ps) to nanosecond (ns) time scale,[26] were obtained at 14.1 T (600 MHz $^{1}$H frequency) using the pulse schemes of Kay and co-workers.[44] The $R_1$ and $R_2$ measurements employed recycle delays of 1.2 s. For the $R_1$ measurements, $^{15}$N−$^{1}$H correlation spectra were collected with longitudinal relaxation delays of 5, 65, 145, 245, 365, 525, 750, and 1150 ms, and for the $R_2$ measurements a Carr−Purcell−Meiboom−Gill (CPMG) $\pi$-pulse train was applied on the $^{15}$N channel during transverse relaxation delays of 7.2, 21.6, 43.2, 57.6, 72, 108, and 144 ms. For the $\{^{1}H\}-^{15}N$ NOE measurements, the reference and NOE spectra were acquired by using a 5 s relaxation delay and a 1 s relaxation delay followed by a 4 s proton presaturation period, respectively.

Measurements of $\eta_{xy}$, the $^{1}$H−$^{15}$N dipole−dipole/$^{15}$N chemical shift anisotropy (CSA) interference rate constant for transverse $^{15}$N magnetization,[45,46] were carried out at 14.1 T using the pulse scheme described by Palmer and co-workers[46] with recycle delays of 2.5 s and used to assess the extent of chemical exchange at different protein sites.[24,47,48] The measurements employed relaxation periods $T$ of 32.0, 53.4, 74.8, and 106.8 ms. The ratios of spectral intensities obtained from separate experiments that detect either the in-phase ($N_y$) or antiphase ($2H_zN_y$) $^{15}$N magnetization were used to calculate the residue-specific $\eta_{xy}$ values according to[45]

$$\frac{\langle N_y(T)\rangle}{\langle 2H_zN_y(T)\rangle} = \tanh(\eta_{xy}T) \quad (1)$$

Quantitative studies of protein conformational dynamics on the millisecond (ms) time scale were undertaken using CPMG relaxation dispersion NMR techniques,[25,28,29] with data collected at magnetic field strengths of 14.1 and 18.8 T, corresponding to $^{1}$H frequencies of 600 and 800 MHz, respectively. A constant-time, relaxation-compensated pulse sequence developed by Kay and co-workers,[49] with a $^{1}$H continuous wave spin-lock field applied during the $^{15}$N CPMG $\pi$-pulse train, was used. Spectra were recorded in an interleaved manner with a constant relaxation delay $T_{relax}$ = 30 ms and a $^{15}$N CPMG $\pi$-pulse width $t_{180,N}$ = 90 μs. The number of $^{15}$N CPMG $\pi$-pulses applied during the $T_{relax}$ period determined the CPMG frequency, $\nu_{CPMG}$, according to[49]

$$\nu_{CPMG} = \frac{1}{2(2\tau_{CP} + t_{180,N})} \quad (2)$$

where $2\tau_{CP}$ is the spacing between successive $^{15}N$ CPMG $\pi$-pulses. In our experiments $\nu_{CPMG}$ was varied between 33.33 and 1000 Hz. The $^{1}H$ spin-lock fields used were in the 8.5−11 kHz range, with the exact RF amplitude fine-tuned for each $\nu_{CPMG}$ value to ensure that an integral number of $^{1}H$ $\pi$-pulses are accommodated within $T_{relax}$, and an equilibration delay $\tau_{eq}$ = 5 ms was used before and after the water alignment as recommended.[49] For each data set, a total of 22−24 $^{15}N-^{1}H$ correlation spectra, corresponding to different $\nu_{CPMG}$ values, were recorded. This included two sets of triplicate measurements—one for a relatively low CPMG frequency ($\nu_{CPMG}$ = 100 Hz) and the other for a high CPMG frequency ($\nu_{CPMG}$ = 800−1000 Hz)—as well as one control experiment with no CPMG relaxation delay (i.e., $T_{relax}$ = 0). The $^{15}N-^{1}H$ spectra were collected with a recycle delay of 3 s and a total experiment time of ∼48−60 h per data set. For each backbone amide $^{15}N$ the effective transverse relaxation rate, $R_{2,eff}$, as a function of $\nu_{CPMG}$ was calculated as[50,51]

$$R_{2,\,\mathrm{eff}}(\nu_{CPMG}) = -\frac{1}{T_{relax}} \ln\left[\frac{I(\nu_{CPMG})}{I_0}\right] \qquad (3)$$

where $T_{relax}$ is the fixed 30 ms relaxation delay, $I(\nu_{CPMG})$ is the peak intensity for a particular CPMG frequency, and $I_0$ is the peak intensity in the control spectrum recorded with $T_{relax}$ = 0.

**NMR Data Processing, Analysis, and Modeling.** All NMR spectra used to extract the protein motional parameters were processed in NMRPipe[52] with Lorentzian-to-Gaussian apodization. Peak intensities were obtained by fitting the spectra to Gaussian lineshapes using the nlinLS routine in NMRPipe.

For the $R_1$ and $R_2$ experiments, the relaxation trajectories were modeled as single-exponential decays to extract the residue-specific relaxation rate constants. The site-resolved $\{^{1}H\}-^{15}N$ NOEs were obtained as ratios of cross-peak intensities determined in the presence and absence of the presaturation pulses. Errors in $R_1$, $R_2$, and NOE parameters were estimated using the root-mean-square (rms) spectral noise obtained in NMRPipe. For modeling the ps−ns time scale protein backbone dynamics, an initial rotational correlation time estimate for LEN was obtained from the $^{15}N$ $R_2/R_1$ ratios[53] by using the *r2r1_tm* program kindly provided by Dr. Arthur G. Palmer (Columbia University).[54] Subsequently, the rotational diffusion tensor was estimated using the method of Tjandra et al.,[55] implemented in the *r2r1_diffusion* program.[54] This calculation utilized the rotational correlation time estimate obtained above and the X-ray structure of LEN (PDB entry 1LVE),[56] which was used to construct the LEN dimer and appropriately rotated and translated with the *pdbinertia* program.[54] For this initial estimation of the diffusion tensor only residues located in the $\beta$-strands of LEN were considered; furthermore, from this subset of residues we excluded those displaying elevated fast internal motions (characterized by $\{^{1}H\}-^{15}N$ NOE values of <0.7) or significant chemical exchange contributions to $R_2$ according to the CPMG relaxation dispersion measurements (*vide infra*).[55] An *F*-value analysis was used to select the appropriate model for the diffusion tensor. This diffusion tensor estimate was then used as the input for an initial round of Lipari−Szabo model-free analysis,[57,58] followed by the simultaneous optimization of both the diffusion tensor and model-free parameters. This process was iterated within the *FASTModelFree*[59] implementation of the *ModelFree* program[60,61] until a self-consistent set of parameters was obtained. All model-free calculations assumed an N−H bond length of 1.02 Å and an $^{15}N$ CSA of −160 ppm.

For the CPMG relaxation dispersion experiments, uncertainties in the measured $R_{2,eff}$ values for each residue were calculated according to $\Delta R_{2,eff}(\nu_{CPMG}) = (1/T_{relax})[\Delta I/I(\nu_{CPMG})]$,[51] where $\Delta I$ is the average standard deviation in the peak intensity estimated from the two sets of triplicate measurements described above. In cases where $\Delta R_{2,eff}$ was found to be less than 2% of the corresponding $R_{2,eff}$, a minimum value of 2% was imposed for the subsequent calculations.[51] The residue-specific CPMG relaxation dispersion trajectories were obtained by plotting $R_{2,eff}$ vs $\nu_{CPMG}$, and data from both magnetic field strengths were fit simultaneously to the Carver−Richards model for two-site exchange[62] using the *CPMGfit* program kindly provided by Dr. Arthur G. Palmer.[54] Results of this calculation were used to perform an initial identification of backbone amide $^{15}N$ spins subject to chemical exchange as follows. For each residue, the simulated CPMG relaxation dispersion trajectories at 600 and 800 MHz $^{1}H$ frequency were used to calculate the corresponding exchange contributions to $^{15}N$ $R_2$ according to $R_{ex} = R_{2,eff}(\nu_{CPMG} = 0) - R_{2,eff}(\nu_{CPMG} = 1000)$; residues with $R_{ex} > 3\ s^{-1}$ at 600 MHz were classified as exhibiting significant chemical exchange, while those with $R_{ex} < 3\ s^{-1}$ were assumed to display negligible motions on the ms time scale. This analysis identified several contiguous regions of ∼5−20 residues in LEN, displaying elevated chemical exchange. For each of these regions, the 600 and 800 MHz CPMG relaxation dispersion trajectories were used simultaneously to perform independent global two-state fits within the *Catia* program kindly provided by Dr. Lewis E. Kay (University of Toronto).[63] These calculations yielded the exchange parameters for each region, including the exchange rate between the two conformers ($k_{ex}$), the population of the minor conformer ($p_B$), and the absolute values of residue-specific chemical shift differences between the two exchanging states ($|\Delta\omega|$). Calculations were performed with an array of starting values for $k_{ex}$ and $p_B$. For each region the final $k_{ex}$ and $p_B$ parameters and their uncertainties were obtained as the averages of the corresponding values in the 20 lowest $\chi^2$ fits. The $|\Delta\omega|$ value for each residue was subsequently recalculated using these mean $k_{ex}$ and $p_B$ parameters. The robustness of the fits and extracted exchange parameters was verified by removing trajectories for individual residues from the data set, re-estimating $k_{ex}$, $p_B$, and $|\Delta\omega|$ and comparing the resulting values to the exchange parameters obtained using the complete data sets. The signs of chemical shift differences between the major and minor conformers were subsequently determined by comparing the $^{15}N$ chemical shifts in a pair of HSQC and heteronuclear multiple quantum coherence (HMQC) spectra recorded at 800 MHz $^{1}H$ frequency as described by Skrynnikov et al.,[64] with shift differences ≥0.3 Hz being considered significant for the accurate prediction of signs.

## RESULTS

**Effect of pH on LEN Backbone Chemical Shifts and Secondary Structure.** A series of 2D $^{15}N-^{1}H$ HSQC spectra of LEN were recorded at pH values ranging from 2.0 to 7.4 as described in the Experimental Procedures section. LEN is a soluble dimer at around physiological pH and is known to form amyloid fibrils at low pH under agitation.[18−21] The complete backbone and side-chain resonance assignments of LEN at pH 6.5 have been established previously,[40] and an assigned HSQC spectrum under these conditions is shown in Figure 1a (blue contours). The spectra of LEN at pH values between 7.4 and 5.2 were found to be virtually superimposable. Upon further

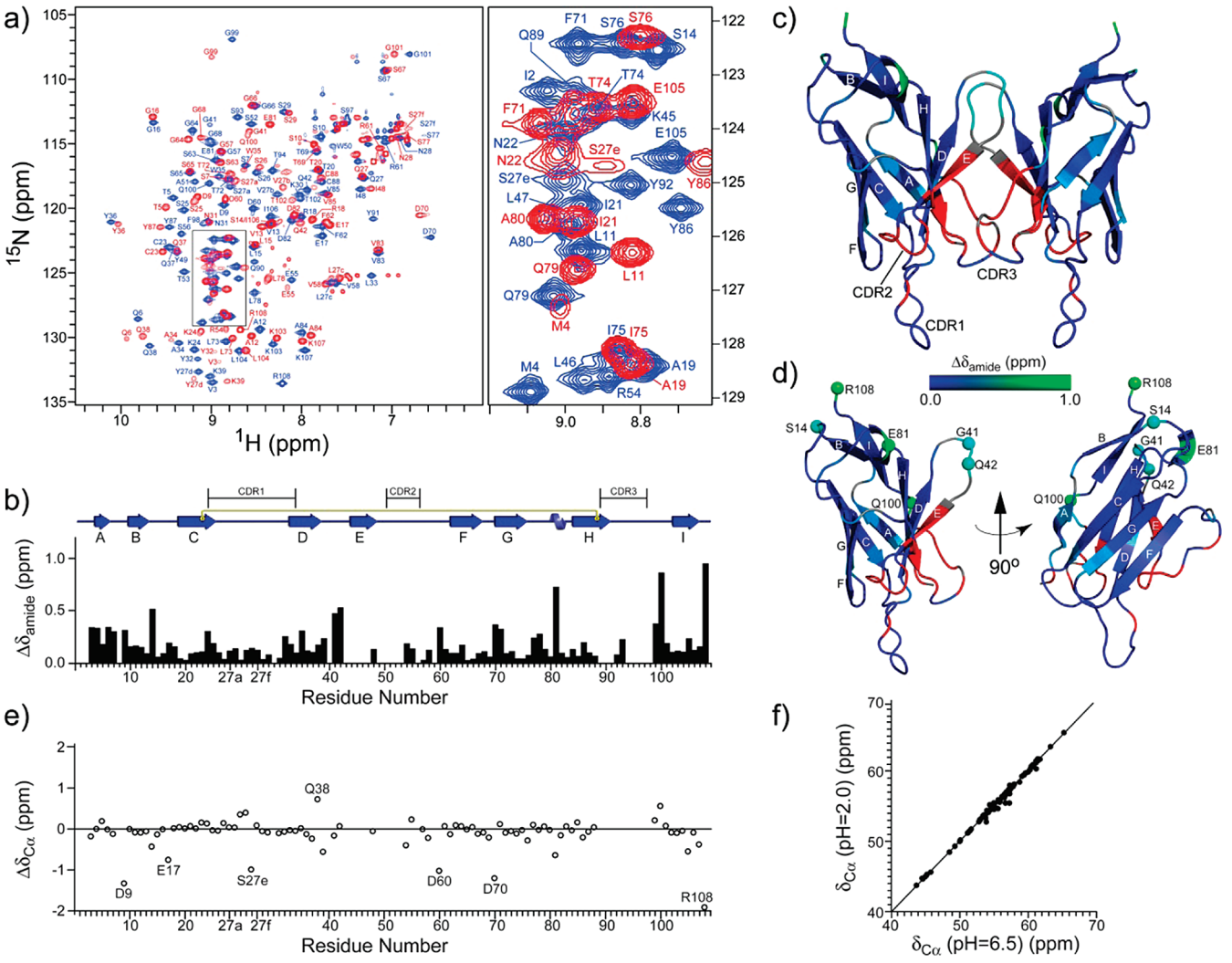


**Figure 1.** Comparison of NMR chemical shifts for LEN at pH 6.5 and 2.0. (a) 800 MHz $^{15}$N−$^{1}$H HSQC spectra of LEN at pH 6.5 (blue contours) and 2.0 (red contours), with the backbone resonance assignments indicated. (b) Plot of residue-specific amide chemical shift changes($\Delta\delta_{amide}$= $[(\Delta\delta_{HN})^2 + (\Delta\delta_N/5)^2]^{1/2}$, where $\Delta\delta_{HN}$ and $\Delta\delta_N$ are the changes in $^{1}H^N$ and $^{15}$N chemical shifts, respectively) observed for LEN upon changing the pH from 6.5 to 2.0. (c, d) Amide chemical shift changes from panel (b) mapped onto the X-ray structure of (c) the LEN dimer and (d) one of the monomer subunits (PDB entry 1LVE). The observed $\Delta\delta_{amide}$ values range from ∼0 ppm (blue) to ∼1 ppm (green), as indicated by the color bar. The N-terminal residue (D1) and six prolines (aa 8, 40, 43, 44, 59, 95), which are undetectable in $^{15}$N−$^{1}$H HSQC spectra, are colored in gray, while residues for which a $\Delta\delta_{amide}$ value could not be determined due to excessive chemical exchange broadening in pH 6.5 and/or 2.0 spectra are colored in red. The average $\Delta\delta_{amide}$ was found to be 0.17 ± 0.17 ppm, and residues with $\Delta\delta_{amide}$ > 0.4 ppm are indicated by spheres and labeled accordingly. (e) Plot of residue-specific $^{13}C^{\alpha}$ chemical shift differences for LEN at pH 6.5 and 2.0 ($\Delta\delta_{C\alpha} = \delta_{C\alpha}$(pH = 2.0) − $\delta_{C\alpha}$(pH = 6.5)), where $\delta_{C\alpha}$ are the observed $^{13}C^{\alpha}$ chemical shifts at the pH value indicated). The average $\Delta\delta_{C\alpha}$ is −0.1 ± 0.4 ppm, and the largest outliers are labeled by residue number. (f) Plot of $^{13}C^{\alpha}$ shifts for LEN at pH 2.0 vs pH 6.5 (the linear correlation coefficient squared was found to be $r^2$ = 0.991).

reduction of pH, to as low as ∼2, small changes in many backbone amide chemical shifts were observed, with the most pronounced changes occurring at pH ∼3−4 (Supporting Information Figure S1). These low pH-induced chemical shift changes were completely reversible upon returning the pH value back to ∼7.

The 2D $^{15}$N−$^{1}$H HSQC spectrum of LEN at pH 2.0 (Figure 1a, red contours) could be largely assigned from the pH titration experiments. However, in order to confirm these resonance assignments and unambiguously assign the remaining amide signals (as well as establish the $^{13}C^{\alpha}$ chemical shifts), a 3D HNCA spectrum of $^{13}$C,$^{15}$N-LEN at pH 2.0 was also recorded (data not shown). Altogether, backbone amide $^{15}$N−$^{1}$H correlations for 89 of 108 non-proline residues could be unambiguously assigned for LEN at pH 2.0. The 19 non-proline residues that could not be assigned include D1, I2, K30, K45-L47, Y49-T53, S56, Q89-Y91, T94, and Y96-F98. These residues, the majority of which are found in complementarity determining (CDR) loop regions 2 and 3 near the LEN dimer interface, were broadened beyond detection at low pH most likely due to significant conformational exchange dynamics as discussed below. Interestingly, a number of the same residues were also found to exhibit pronounced exchange broadening at pH 6.5.[40]

For each residue in LEN that could be assigned in the pH 6.5 and 2.0 $^{15}$N−$^{1}$H HSQC spectra, the overall change in amide chemical shift was obtained from the expression

$$\Delta\delta_{amide} = \sqrt{(\Delta\delta_{HN})^2 + (\Delta\delta_N/5)^2} \quad (4)$$


dx.doi.org/10.1021/bi200410c |*Biochemistry* 2011, 50, 5845–5857

where $\Delta\delta_{HN}$ and $\Delta\delta_N$ are the observed differences in the $^1H^N$ and $^{15}N$ chemical shifts, respectively, between the pH 6.5 and 2.0 spectra. By and large, the perturbations in backbone amide chemical shifts of LEN upon acidification were found to be relatively minor, with the average $\Delta\delta_{amide}$ of 0.17 ± 0.17 ppm and only six residues (S14, G41, Q42, E81, Q100, and R108) with $\Delta\delta_{amide}$ > 0.4 ppm. Figure 1b shows the plot of $\Delta\delta_{amide}$ vs residue number, and in Figure 1c,d the amide chemical shift changes are mapped onto the X-ray structure of LEN. These results suggest that LEN does not undergo major structural changes between physiological and acidic pH.

To probe more directly for the presence of pH-related structural differences in LEN, we also examined the pH dependence of $^{13}C^\alpha$ shifts, which are highly sensitive reporters of the protein backbone conformation.[65] Figure 1f shows that $^{13}C^\alpha$ shifts at pH 6.5 and 2.0 exhibit a nearly linear correlation ($r^2$ = 0.991). Calculation of residue-specific $^{13}C^\alpha$ shift differences, $\Delta\delta_{C\alpha} = \delta_{C\alpha}(pH = 2.0) - \delta_{C\alpha}(pH = 6.5)$, yields an average $\Delta\delta_{C\alpha}$ of −0.1 ± 0.4 ppm and shows that nearly all of the few outliers characterized by $|\Delta\delta_{C\alpha}|$ in the ∼1−2 ppm range (Figure 1e) correspond to loop regions and amino acid residues having carboxylate groups (Asp, Glu, C-terminus) that become protonated at low pH. Taken together, the comparison of backbone $^1H^N$, $^{15}N$, and $^{13}C^\alpha$ chemical shifts at pH 6.5 and 2.0 strongly indicates that the three-dimensional fold of LEN remains effectively unperturbed upon acidification. This is consistent with previous suggestions by Fink and co-workers,[19−21] based on results of low-resolution biophysical measurements, that structures of LEN at physiological and low pH are similar. Concurrently, the facts that LEN is capable of assembling into amyloid fibrils at pH 2[19−21] and that partial unfolding of proteins is generally believed to be a critical step in amyloid formation[1,2] imply that thorough knowledge of LEN dynamics is likely to be important for understanding the initial steps along the protein aggregation pathway. With this premise we have commenced a comparative study of the backbone dynamics of LEN at physiological and acidic pH.

**Fast Time Scale Protein Backbone Dynamics.** The ps−ns time scale dynamics of LEN were probed at pH 6.5 and 2.0, by measuring the $R_1$ and $R_2$ rates and $\{^1H\}-^{15}N$ NOEs for backbone amide $^{15}N$ nuclei (Supporting Information Table S1 and Figure S2). At pH 6.5, relaxation data could be obtained for 103 of 108 nonproline residues. (Data for D1, S27f, Q37, L47, and Y96 were not accessible due to excessive exchange broadening or peak overlap in 2D $^{15}N-^1H$ HSQC spectra.) In order to extract quantitative motional parameters from these data, the extended Lipari−Szabo model-free formalism was employed,[57,58,66] and the analysis was performed using isotropic and anisotropic motional models. While a reasonable fit to the experimental data could be obtained with an isotropic tumbling model, the statistical *F*-value analysis clearly indicated an axially symmetric anisotropic rotational diffusion model to be more appropriate; the use of a fully asymmetric diffusion tensor did not provide a further statistically significant improvement to the fit. As noted in the Experimental Procedures section, the initial rotational diffusion tensor parameters were estimated according to an established approach,[55] with $^{15}N$ $R_2/R_1$ ratios for a conservative set of 40 residues located in the most highly structured $\beta$-strand regions of the protein and the X-ray structure of LEN used to construct the dimer. Model-free calculations were then initiated for the 103 residues with available relaxation data, with concurrent optimization of the diffusion tensor parameters. In summary, the model-

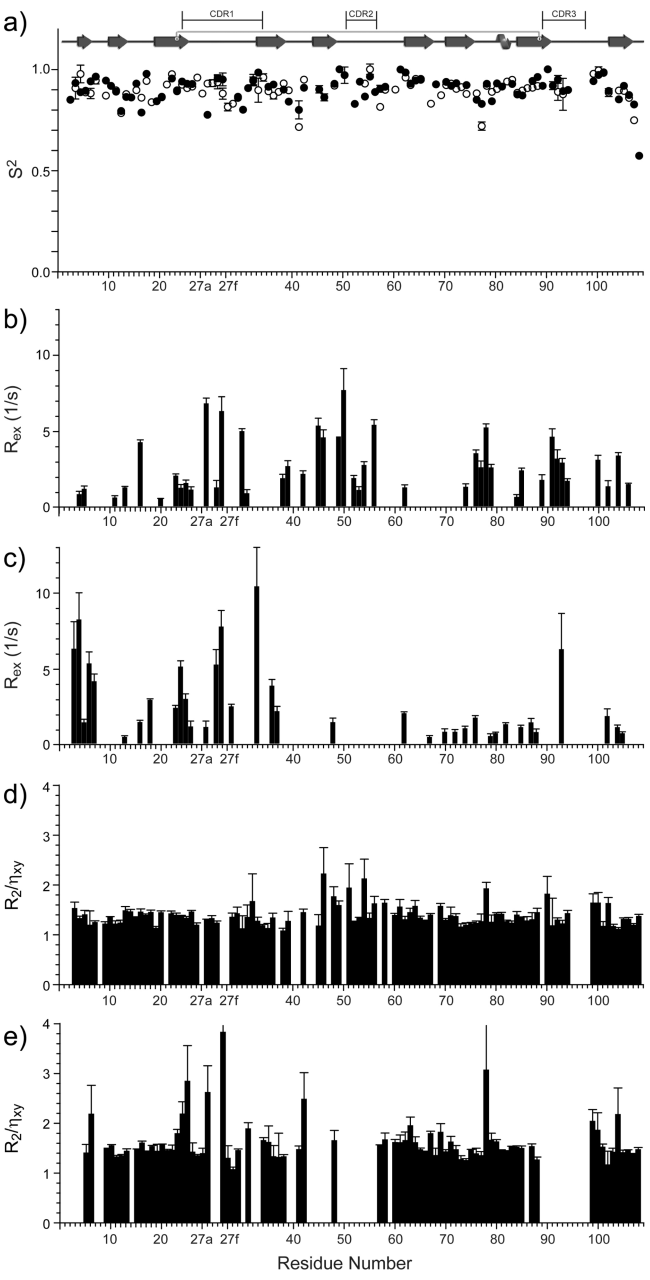


**Figure 2.** Model-free analysis of picosecond−nanosecond time scale protein backbone motions and qualitative characterization of slower time scale dynamics for LEN at pH 6.5 and 2.0. (a) Generalized backbone amide order parameters, $S^2$, for LEN at pH 6.5 (filled circles) and pH 2.0 (hollow circles) obtained by fitting $^{15}N$ spin relaxation ($R_1$, $R_2$, and NOE) data at 600 MHz $^1H$ frequency to one of the five possible motional models according to Mandel et al.[60] (see text and Supporting Information Tables S1 and S2 and Figure S2 for additional details). (b, c) Plots of phenomenological chemical exchange correction factors, $R_{ex}$, required to properly account for the experimental $^{15}N$ $R_2$ values within model-free analysis for LEN at pH 6.5 (b) and pH 2.0 (c). (d, e) Plots of $R_2/\eta_{xy}$, the ratio of the $^{15}N$ transverse relaxation rate constant to the $^1H-^{15}N$ dipole−dipole/$^{15}N$ CSA interference rate constant, determined at 600 MHz $^1H$ frequency for LEN at pH 6.5 (d) and 2.0 (e). The average $R_2/\eta_{xy}$ values were found to be 1.38 ± 0.21 at pH 6.5 and 1.6 ± 0.4 at pH 2.0; for residues that are not subject to slow conformational exchange $R_2/\eta_{xy}$ is expected to be approximately constant (see text for additional details).

free analysis yielded generalized order parameters, $S^2$, for 84 residues (Supporting Information Table S2) with an average $S^2$ of 0.90 ± 0.06, as well as the diffusion tensor parameters including the rotational correlation time, $\tau_c$, of 13.48 ± 0.01 ns and $D_\parallel/D_\perp$ = 0.825 ± 0.006. The remaining 19 residues could not be satisfactorily assigned to any one of the five possible motional models.[60]

A similar analysis of fast time scale motions was performed using $^{15}$N $R_1$, $R_2$, and $\{^1H\}-^{15}N$ NOE data for LEN at pH 2.0 (Table S1 and Figure S2). In this case an axially symmetric diffusion tensor was also found to provide the best fit to the relaxation measurements, with the final optimized parameters $\tau_c$ = 13.42 ± 0.01 ns and $D_\parallel/D_\perp$ = 0.880 ± 0.005. Note that the diffusion tensor estimation assumed that the fold of LEN at pH 2.0 is accurately represented by the X-ray structure under native conditions; this assumption appears to be reasonable based on the backbone chemical shift data discussed above. In summary, order parameters were obtained for a total of 78 residues (Table S2) with an average $S^2$ of 0.90 ± 0.05; ten residues could not be assigned to any of the five motional models, and relaxation data could not be accurately extracted for S14 due to partial peak overlap in the HSQC spectra.

The comparative analysis of ps−ns time scale dynamics of LEN at pH 6.5 and 2.0 allows several conclusions to be made. First, we note that $^{15}$N $R_1$, $R_2$, and $\{^1H\}-^{15}N$ NOE measurements at both pH values are optimally fit with effectively identical diffusion tensor parameters and that the calculated $\tau_c$ values are characteristic of the presence of a predominantly dimeric protein species. In other words, the native three-dimensional fold and oligomeric state of LEN are not significantly altered at low pH. Second, the residue-specific order parameters obtained using the model-free approach (Figure 2a) reveal that, on the whole, the LEN backbone does not undergo significant motions on the ps−ns time scale irrespective of pH, with the average $S^2$ of ∼0.9 at both pH 6.5 and 2.0. We note, however, that a small number of residues in LEN at pH 6.5 (A12, S14, A19, S29, E81, V83, K107, and R108) and pH 2.0 (A12, L15, G41, S77, I106, and K107) do appear to experience elevated internal motions on the ∼500−2000 ps time scale (Table S2). Most of these residues (except S29 and G41) are located at the periphery of the LEN dimer near the C-termini and are thus unlikely to be of major functional relevance. Third, and most significantly, the model-free calculations for LEN at both pH values required the inclusion of phenomenological chemical exchange correction factors ($R_{ex}$) in order to adequately model the $^{15}$N $R_2$ relaxation data for a number of residues. As shown in Figure 2b, at physiological pH, residues that display increased likelihood of undergoing chemical exchange dynamics are located primarily in the three CDR loops. At pH 2.0 the largest exchange contributions to $R_2$ were found for residues in the N-terminal β-strand and the CDR1 region (Figure 2c), while a number of residues in the CDR2 and CDR3 regions exhibited severe exchange broadening and were not detectable in HSQC spectra. These observations point to the possible presence in LEN of slower time scale conformational dynamics, which become more pronounced at acidic pH. Motions of this type are frequently associated with partial unfolding of proteins[29] and are therefore likely to be relevant for understanding protein aggregation phenomena. The fact that no doubling of backbone amide resonances is readily detected in HSQC spectra of LEN at either pH suggests that populations of the minor protein conformers are relatively low and/or that exchange dynamics are in the fast or intermediate regime on the chemical shift time scale. Consequently, we have focused our attention on the characterization of the slower, ms time scale backbone dynamics of LEN as a function of pH.

**Characterization of Slow Time Scale Protein Motions.** Prior to quantitative analysis of ms time scale backbone dynamics by CPMG relaxation dispersion NMR techniques, measurements of $^1H-^{15}N$ dipole−dipole/$^{15}$N CSA interference rate constants, $\eta_{xy}$, were performed for LEN at pH 6.5 and 2.0 (Table S1 and Figure S2). In the absence of chemical exchange, $^{15}$N $R_2$ rates are given by $\kappa\eta_{xy}$,[46] where $\kappa$ is a constant characteristic of the protein. Therefore, determination of residue-specific $R_2/\eta_{xy}$ ratios provides a convenient approach to rapidly and directly probe for the presence of slow conformational exchange along the protein backbone—namely, assuming that most sites are relatively unaffected by chemical exchange phenomena, the aa residues with considerably elevated $R_2/\eta_{xy}$ ratios with respect to the average are likely to be subject to significant dynamics on the ms time scale.[24] At pH 6.5, most residues in LEN display very similar $R_2/\eta_{xy}$ ratios (Figure 2d), with the average value of 1.38 ± 0.21. A total of 12 residues, including Y32, L46, I48, A51, R54, S56, V58, L78, Q90, G99, Q100, and T102, have $R_2/\eta_{xy}$ ratios of at least one standard deviation larger than the average. For LEN at pH 2.0, the $R_2/\eta_{xy}$ average and dispersion (1.6 ± 0.4) both increased compared to pH 6.5, with Q6, K24, S25, V27b, S27e, Q42, L78, G99, and L104 having $R_2/\eta_{xy}$ ratios of at least one standard deviation larger than the mean. Although qualitative, the $R_2/\eta_{xy}$ analysis confirms that multiple residues in LEN, many located in or around the CDR loop regions, indeed experience exchange dynamics at pH 6.5 and pH 2.0 and that these effects appear to become more pronounced as the pH is decreased.

Millisecond time scale motions of LEN were subsequently examined quantitatively by using $^{15}$N-CPMG relaxation dispersion NMR methods, which are able to probe chemical exchange phenomena in proteins that involve minor conformer populations on the order of a few percent or less.[28,29] Residue-specific relaxation dispersion trajectories at magnetic field strengths of 14.1 and 18.8 T were recorded for LEN at pH 6.5 and 2.0. Initially, the relaxation dispersion data for individual residues were fit to the Carver−Richards model for two-site exchange[62] to obtain estimates for the chemical exchange contribution, $R_{ex}$, to $^{15}$N $R_2$. Figures 3a and 3c show plots of $R_{ex}$ at 600 and 800 MHz $^1$H frequency as a function of residue number for LEN at pH 6.5 and 2.0, respectively. In Figures 3b and 3d, the $R_{ex}$ values at 600 MHz and pH 6.5 and 2.0, respectively, are mapped onto the X-ray structure of LEN. At pH 6.5, the vast majority of residues characterized by $R_{ex} > 3$ s$^{-1}$ at 600 MHz and interpreted as undergoing significant exchange dynamics (Figures 3a and 3b) were found to cluster roughly in three contiguous stretches: (1) aa V3-D9 near the N-terminus (denoted "region 1" and containing β-strand A), (2) aa Q42-G57 (denoted "region 2" and encompassing β-strand E and the entire CDR2 loop), and (3) aa Q89-G101 (denoted "region 3" and containing the CDR3 loop). Note that several isolated residues within these dynamic stretches (e.g., S52) displayed relatively low $R_{ex}$ values—this is likely due to similar chemical shifts for the exchanging conformers (*vide infra*). On the other hand, large segments of the protein backbone, spanning residues ∼10−35 and ∼60−85 as well as ∼5−6 C-terminal amino acids, exhibit generally negligible ms time scale motions. Analogous studies at acidic pH reveal that all LEN residues in regions 1−3 subject to chemical exchange at pH 6.5 are also dynamic at pH 2.0, with the majority

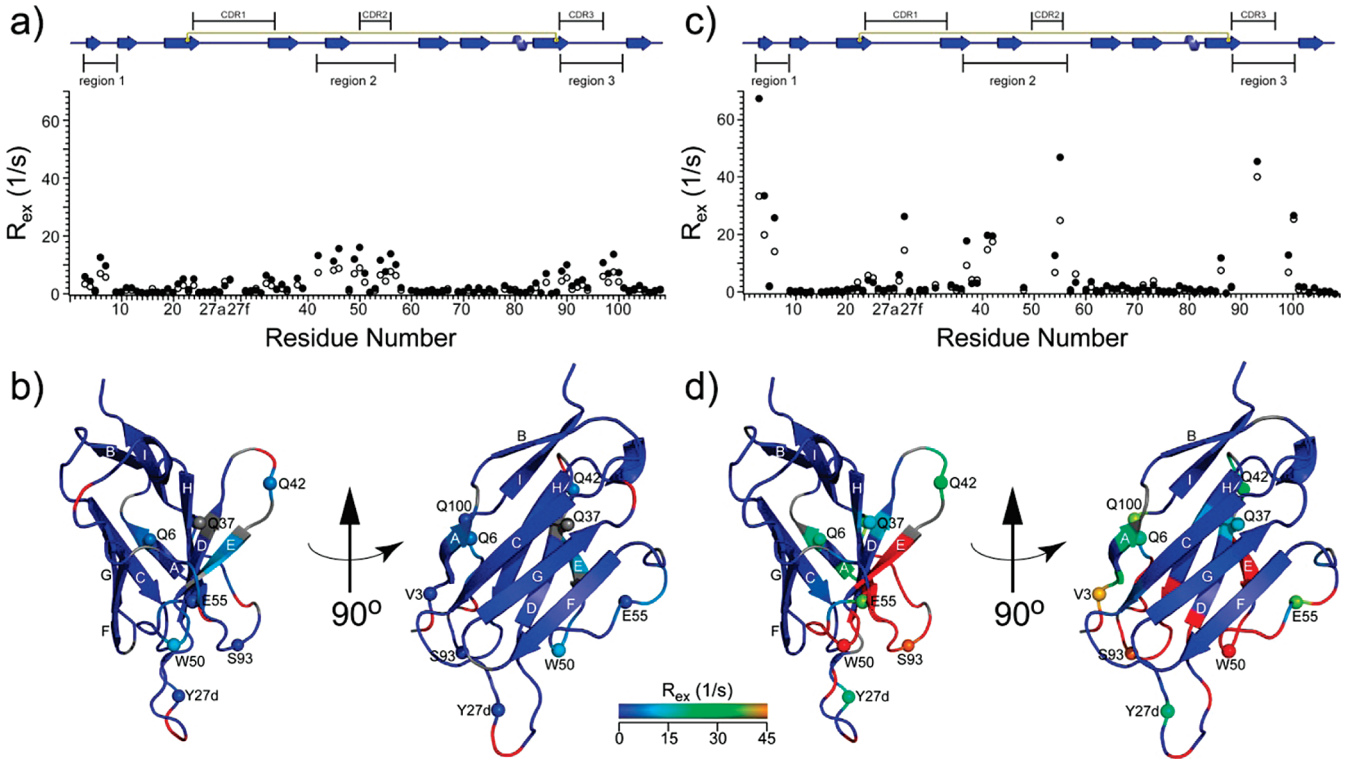


**Figure 3.** Summary of $^{15}$N-CPMG relaxation dispersion NMR data for LEN at pH 6.5 and 2.0. (a) Plot of $R_{ex}$, the estimated chemical exchange contribution to $^{15}$N $R_2$, for LEN at pH 6.5 and 14.1 T (hollow circles) and 18.8 T (filled circles). The $R_{ex}$ values for individual residues were determined as described in the text, by simultaneously fitting the CPMG relaxation dispersion trajectories (obtained by plotting the effective $^{15}$N $R_2$ rate vs CPMG frequency) at both magnetic fields to the Carver−Richards model for two-site exchange. The simulated trajectories were used to calculate $R_{ex}$ according to $R_{ex} = R_{2,eff}(\nu_{CPMG} = 0) - R_{2,eff}(\nu_{CPMG} = 1000)$, where $R_{2,eff}(\nu_{CPMG} = 0)$ and $R_{2,eff}(\nu_{CPMG} = 1000)$ are the effective $^{15}$N $R_2$ rates at 0 and 1000 Hz CPMG frequency, respectively; residues with $R_{ex} > 3$ s$^{-1}$ at 14.1 T were interpreted to exhibit significant motions on the ms time scale. (b) The $R_{ex}$ values at 14.1 T mapped onto the X-ray structure for one of the monomer subunits of LEN, with magnitudes indicated by the color bar. Residues that were undetectable or displayed severe peak overlap in the $^{15}$N−$^{1}$H HSQC spectrum are colored in gray, while residues for which $R_{ex}$ could not be determined due to excessive chemical exchange broadening are colored in red. For reference, the $\beta$-strands of LEN have been labeled (cf. Figure 1), and several residues with elevated $R_{ex}$ values, located primarily in dynamic regions 1−3 highlighted in the wiring diagram in panel (a), have been explicitly indicated by spheres. (c, d) Same as panels (a, b) for LEN at pH 2.0.

characterized by much larger $R_{ex}$ values, or cannot be detected at all in HSQC spectra due to excessive exchange broadening (Figures 3c and 3d). Several additional residues, most found in the vicinity of region 2 and a few isolated aa in the CDR1 loop, also showed elevated $R_{ex}$ values relative to pH 6.5. In summary, the quantitative CPMG relaxation dispersion measurements reveal that residues located near the N-terminus of LEN as well as in and around the CDR2 and CDR3 loops in proximity of the dimer interface are subject to considerable ms time scale dynamics, which become more significant at low pH. Meanwhile, for the most part, the structured $\beta$-sheet core region of the protein and the CDR1 loop experience minimal conformational flexibility. These findings are generally in agreement with the more qualitative evaluation of chemical exchange phenomena by the model-free and $R_2/\eta_{xy}$ approaches discussed above.

In order to extract the rates of exchange between the major and minor protein conformers, $k_{ex}$, within the two-site exchange model, and the populations of minor conformers, $p_B$, from the CPMG relaxation dispersion trajectories, we performed global two-state fits of data at both magnetic fields for residues located in regions 1−3 identified above. Initial data fitting was done by assuming the same $k_{ex}$ and $p_B$ parameters for all three dynamic regions of LEN at each pH—this analysis yielded $k_{ex} = 491 \pm 19$ s$^{-1}$ and $p_B = 2.40 \pm 0.10\%$ at pH 6.5 and $k_{ex} = 500 \pm 13$ s$^{-1}$ and $p_B = 6.84 \pm 0.11\%$ at pH 2.0. Although, on the whole, reasonable quality fits to the relaxation dispersion data were obtained in this manner, it was also apparent that trajectories showing the largest relaxation dispersion were fit quite poorly, especially for small $\nu_{CPMG}$ frequencies (data not shown). Experimental data were therefore reanalyzed by considering dynamic regions 1−3 independently from one another, which resulted in significantly improved fits for all relaxation dispersion trajectories (see representative trajectories and fits in Figure 4 and complete data sets in Supporting Information Figures S3 and S4) and yielded independent exchange parameters, $k_{ex}$ and $p_B$, for each region as follows: pH 6.5, region 1: $k_{ex} = 200 \pm 40$ s$^{-1}$, $p_B = 4.0 \pm 0.40\%$; region 2: $k_{ex} = 630 \pm 30$ s$^{-1}$, $p_B = 2.30 \pm 0.06\%$; region 3: $k_{ex} = 250 \pm 30$ s$^{-1}$, $p_B = 2.30 \pm 0.21\%$; pH 2.0, region 1: $k_{ex} = 690 \pm 30$ s$^{-1}$, $p_B = 15.6 \pm 1.8\%$; region 2: $k_{ex} = 540 \pm 20$ s$^{-1}$, $p_B = 11.6 \pm 0.8\%$; region 3: $k_{ex} = 390 \pm 30$ s$^{-1}$, $p_B = 6.6 \pm 0.3\%$. Since the three flexible regions of LEN are well separated from each other in the primary amino acid sequence, even if their motions are correlated it is reasonable to expect that each region may experience conformational dynamics characterized by somewhat different exchange parameters. Analysis of the CPMG relaxation dispersion trajectories also yielded the differences in $^{15}$N chemical shifts between the two exchanging protein states,


dx.doi.org/10.1021/bi200410c |*Biochemistry* 2011, 50, 5845–5857

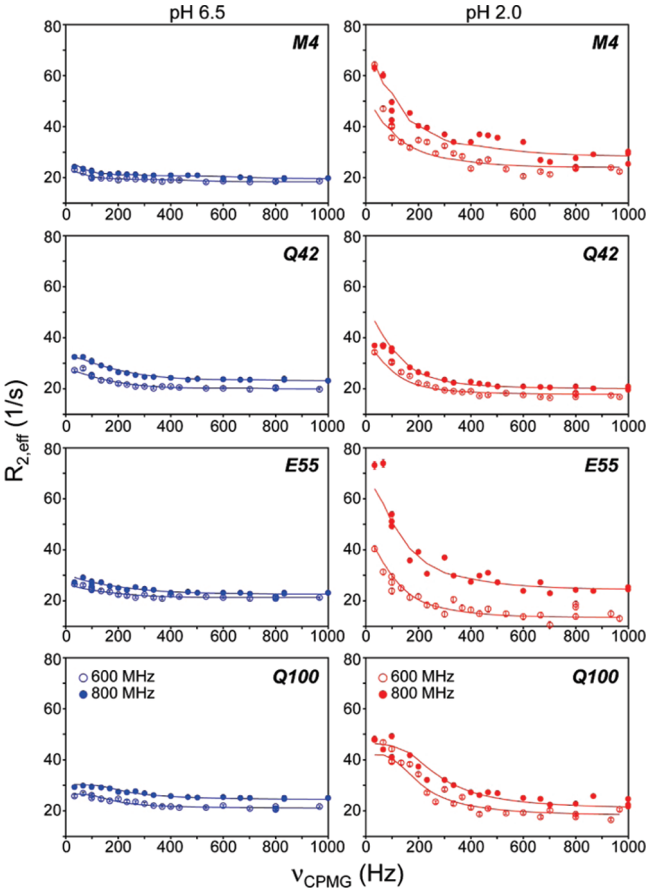


**Figure 4.** $^{15}$N-CPMG relaxation dispersion NMR trajectories for representative residues from the three contiguous regions of LEN exhibiting elevated conformational flexibility on the ms time scale at pH 6.5 and 2.0. Experimental (circles) and simulated (lines) CPMG trajectories at pH 6.5 and 2.0 are shown in blue (left column) and red (right column), respectively, with experimental data corresponding to magnetic field strengths of 14.1 T (600 MHz $^1$H frequency; hollow circles) and 18.8 T (800 MHz $^1$H frequency; filled circles). For each one of the three dynamic regions of LEN (see text and Figure 3 for additional details) the 600 and 800 MHz CPMG trajectories were used simultaneously to perform independent global fits to the two-site exchange model. These calculations yielded the exchange rate between the major and minor conformers ($k_{ex}$), the minor conformer population ($p_B$), and the residue-specific differences in chemical shifts between the two exchanging states ($|\Delta\omega|$) for dynamic regions 1−3 at pH 6.5 and 2.0 (cf. Table 1). The complete set of experimental and simulated CPMG trajectories for the three flexible regions of LEN at pH 6.5 and 2.0 is shown in Supporting Information Figures S3 and S4, respectively.

$\Delta\omega$, for each residue, and these data are summarized in Table 1. At both pH 6.5 and 2.0, most residues for which relaxation data are available exhibit $|\Delta\omega|$ on the order of ∼1 ppm. Given that the exchange rates for dynamic regions 1−3 of LEN are in the ∼200−700 $s^{-1}$ range, these $|\Delta\omega|$ values indicate that the vast majority of residues are in the intermediate ($k_{ex} \sim |\Delta\omega|$) to fast ($k_{ex} > |\Delta\omega|$) exchange regime with respect to $^{15}$N chemical shifts. Thus, the severe line broadening observed at pH 2.0 for multiple residues in flexible regions 2 and 3 is likely caused by increased populations of the minor protein conformers combined with exchange dynamics being in the intermediate regime on the $^{15}$N and/or $^1$H chemical shift time scales.

Taken together, the $^{15}$N relaxation measurements indicate that LEN exhibits limited conformational flexibility with the exception of three well-defined regions of ∼5−20 aa positioned near the dimer interface. Around physiological pH, the slow protein backbone dynamics in these regions are associated with relatively low excited-state protein conformer populations, in the ∼2−4% range. Upon acidification, the CPMG relaxation dispersion data are compatible with a significant, ∼3−4-fold, increase in the higher-energy minor protein conformer populations, accompanied by similar or slightly accelerated rates of exchange between the major and minor conformers for most residues. These findings provide valuable molecular-level insights into why LEN does not form amyloid under physiological conditions and does so only with considerable difficulty at low pH. In addition, our data clearly point to the LEN dimer dissociation process, correlated with increased ms time scale motions for a small set of specific residues, as being one of the important initial steps involved in protein misfolding and amyloid assembly. This conclusion is consistent with the fact that the amide $^{15}$N chemical shifts for many of the dynamic residues in the excited state of LEN, readily obtained from the corresponding major conformer shifts and $\Delta\omega$ values (cf. Table 1), tend toward random coil values.[67]

## DISCUSSION

LEN is structurally homologous to other Ig $V_L$ domains of the $\kappa$ subgroup.[56] The protein fold consists of two antiparallel $\beta$-sheets—made up of strands A, C, G, F and D, E, H (Figure 1) — comprising the framework region and three hypervariable CDR loops located between strands C and D (CDR1), E and F (CDR2), and H and I (CDR3). The tertiary structure is stabilized by hydrogen bonds between the antiparallel strands and the shielding of hydrophobic $\beta$-sheet residues from solvent. Formation of dimeric quaternary structure is facilitated primarily by two sets of intermolecular hydrogen bonds involving side chains of residues Q38 and Q38, and Y36 and Q89,[56] while intramolecular contacts between the Q38 and Y87 side chains further reinforce the structural integrity of the interface region (see Figure 5a). This architecture balances the electrostatic interactions involving surface residues and minimizes unfavorable interactions of nonpolar side chains with water molecules, with contacts between the Q38 side chains being especially important for stabilizing the dimer conformation. In fact, a single mutation, Q38E, has been found to alter the charge balance so severely that a distinct dimer interface is obtained, with one of the monomer subunits rotated by ∼180° relative to the native protein.[68]

At physiological pH LEN does not readily assemble into amyloid fibrils,[6] presumably due to the high degree of stability of the native tertiary and quaternary structure. Indeed, the $^{15}$N relaxation data, which show that overall the LEN dimer displays rather limited backbone motions, are consistent with the notion that the most critical intra- and intermolecular hydrogen-bonding interactions remain effectively intact under these conditions. In spite of this apparent structural integrity, however, the $^{15}$N-CPMG relaxation dispersion measurements reveal the existence of three extended dynamic "hot spots" along the protein backbone, consisting of ∼5−20 amino acids each, subject to slow motions on the ms time scale (Figure 3). These dynamic regions correspond roughly to (1) N-terminal $\beta$-strand A and loop between strands A and B, (2) loop between strands D and E,

**Table 1. Summary of $^{15}$N-CPMG Relaxation Dispersion NMR Data Analysis for the Three Dynamic Regions of LEN at pH 6.5 and 2.0[a]**

| | Δω (ppm) | |
|---|---|---|
| region 1 | pH 6.5, $k_{ex}$ = 200 ± 40 s$^{-1}$, $p_B$ = 4.0 ± 0.4% | pH 2.0, $k_{ex}$ = 690 ± 30 s$^{-1}$, $p_B$ = 15.6 ± 1.8% |
| V3 | −0.99 ± 0.04 | −1.22 ± 0.01 |
| M4 | −0.80 ± 0.03 | −1.13 ± 0.01 |
| T5 | −0.56 ± 0.04[d] | −0.34 ± 0.01 |
| Q6 | −1.26 ± 0.04 | −0.95 ± 0.01 |
| S7 | 1.03 ± 0.04 | −0.74 ± 0.01 |
| D9 | −0.18 ± 0.09[d] | ∼0 |
| | Δω (ppm) | |
| region 2 | pH 6.5, $k_{ex}$ = 630 ± 30 s$^{-1}$, $p_B$ = 2.30 ± 0.06% | pH 2.0, $k_{ex}$ = 540 ± 20 s$^{-1}$, $p_B$ = 11.6 ± 0.8% |
| Q37 | –[b] | −0.58 ± 0.01[d] |
| Q38 | – | 0.50 ± 0.01 |
| K39 | – | −0.40 ± 0.02 |
| P40 | n/a[c] | n/a |
| G41 | – | −0.70 ± 0.01 |
| Q42 | 1.88 ± 0.04 | −1.08 ± 0.01 |
| P43 | n/a | n/a |
| P44 | n/a | n/a |
| K45 | 1.99 ± 0.06 | n/a |
| L46 | 2.57 ± 0.06 | n/a |
| L47 | n/a | n/a |
| I48 | −0.32 ± 0.07 | 0.20 ± 0.03[d] |
| Y49 | −2.01 ± 0.05 | n/a |
| W50 | 2.82 ± 0.07 | n/a |
| A51 | 1.19 ± 0.04 | n/a |
| S52 | ∼0 | n/a |
| T53 | −0.48 ± 0.06 | n/a |
| R54 | 1.78 ± 0.04[d] | −0.74 ± 0.01 |
| E55 | 1.21 ± 0.04 | −1.47 ± 0.02 |
| S56 | −2.18 ± 0.06 | n/a |
| G57 | −1.39 ± 0.04 | −0.20 ± 0.02 |
| V58 | – | −0.40 ± 0.01 |
| | Δω (ppm) | |
| region 3 | pH 6.5, $k_{ex}$ = 250 ± 30 s$^{-1}$, $p_B$ = 2.30 ± 0.21% | pH 2.0, $k_{ex}$ = 390 ± 30 s$^{-1}$, $p_B$ = 6.6 ± 0.3% |
| Q89 | −1.13 ± 0.06[d] | n/a |
| Q90 | 1.29 ± 0.07[d] | n/a |
| Y91 | −0.70 ± 0.06[d] | n/a |
| Y92 | −0.84 ± 0.06 | n/a |
| S93 | 1.10 ± 0.06[d] | n/a |
| T94 | −0.74 ± 0.06 | n/a |
| P95 | n/a | n/a |
| Y96 | n/a | n/a |
| S97 | 2.88 ± 0.12 | n/a |
| F98 | −2.02 ± 0.09 | n/a |
| G99 | 1.67 ± 0.07 | −1.10 ± 0.02 |
| Q100 | −2.92 ± 0.15 | 3.30 ± 0.05 |

**Table 1. Continued**

| | Δω (ppm) | |
|---|---|---|
| region 3 | pH 6.5, $k_{ex}$ = 250 ± 30 s$^{-1}$, $p_B$ = 2.30 ± 0.21% | pH 2.0, $k_{ex}$ = 390 ± 30 s$^{-1}$, $p_B$ = 6.6 ± 0.3% |
| G101 | −0.44 ± 0.07[d] | −0.33 ± 0.03 |

[a] The signs of the chemical shift differences were obtained according to the method of Kay and co-workers.[64] [b] Resonance present in spectrum but not included in data fitting due to low $R_{ex}$ value (see Figure 3). [c] Resonance not detectable due to excessive exchange broadening, spectral overlap, or a proline residue. [d] Difference in $^{15}$N resonance frequencies between HSQC and HMQC spectra <0.3 Hz.

β-strand E, and CDR2 loop, and (3) the CDR3 loop. Interestingly, with the exception of residue S27f which is subject to pronounced conformational exchange broadening in $^{15}$N−$^{1}$H HSQC spectra[40] and residues K24, Y27d, Y32, and L33 which show some degree of relaxation dispersion, the large CDR1 loop located at the periphery of LEN is relatively inflexible on the ms time scale. This is likely due to the presence of an extensive network of intramolecular hydrogen bonds involving the backbone $H^N$ and O atoms of residues V27b, Y27d, S29, K30, and Y32 and the N28 and Y32 side chains.[56]

Although quantitative analysis of the CPMG relaxation dispersion data indicates that populations of higher-energy protein states associated with elevated ms regime backbone motions are very low at physiological pH (∼2−4% of the major, ground-state conformer), the location of the three flexible regions within the LEN structure furnishes valuable molecular-level insights into the likely initial events leading to protein misfolding and amyloid assembly under destabilizing conditions. Specifically, dynamic regions 2 and 3 encompass the vast majority of residues lining the dimer interface, and aa V3-D9, making up dynamic region 1, pack directly against region 3 residues ∼S97-G101 (Figure 5a); all three flexible regions are terminated primarily by interactions involving the framework β-strands. Altogether, it is evident that amino acids located in regions 1−3 of LEN discussed above cluster to form a large area predisposed to undergo considerable conformational fluctuations, covering effectively the entire dimer interface (Figure 5b,c). These conformational fluctuations appear to play an important role in destabilizing the native fold of LEN, triggering dimer dissociation and, ultimately, amyloid formation once a sufficiently high concentration of appropriately misfolded protein states is achieved.[1,2]

In order to further probe this issue, an analogous set of $^{15}$N relaxation measurements was performed at pH 2.0, where in the presence of agitation LEN is known to undergo conversion to the amyloid state.[19−21] Measurements of ps−ns time scale dynamics and backbone chemical shifts (Figures 1 and 2) show that, even at low pH where it is capable of forming amyloid, LEN by and large retains its native three-dimensional fold, in agreement with results of previous low-resolution biophysical measurements[19−21] which suggest that the structure and dimeric state of LEN are relatively unperturbed at pH ∼2. Most remarkable, however, are the findings that (1) all residues along the LEN dimer interface found to exhibit slow conformational dynamics at pH 6.5 (as well as several additional amino acids in the CDR1 loop and in the loop between β-strands D and E, bordering region 2) are subject to significant ms time scale motions at pH 2.0 (Figure 3) and (2) partially unfolded, excited-state protein conformer populations increase significantly, from ∼2−4% at physiological pH to

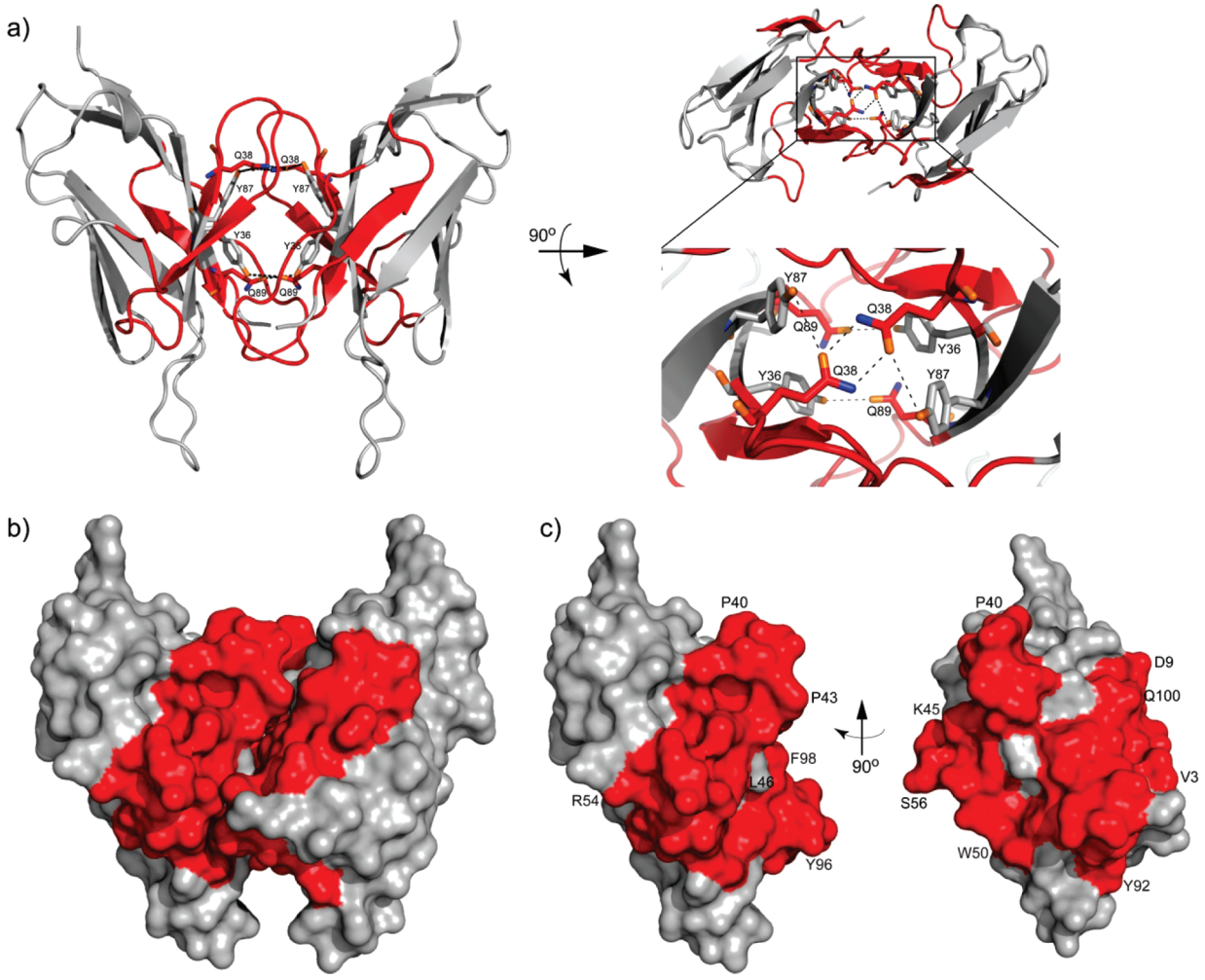


**Figure 5.** Key inter-residue contacts stabilizing the native fold of LEN and summary of the protein regions determined by NMR spectroscopy to undergo the most considerable conformational fluctuations of the backbone atoms on the millisecond time scale. (a) Cartoon representation of the LEN dimer X-ray structure, highlighting important hydrogen-bonding interactions between side chains of residues Y36, Q38, and Q89 across the dimer interface. Residues located in the three contiguous dynamic regions of LEN at pH 6.5 and/or 2.0, as identified by CPMG relaxation dispersion NMR methods (aa 3−9, 37−58, and 89−101; cf. Figure 3 and Table 1) are colored in red. Surface representations of (b) the LEN dimer corresponding to the cartoon diagram in panel (a), and (c) one of the monomer subunits, with the conformationally flexible residues listed above colored in red. Selected residues are labeled for reference.

∼10−15% at low pH. The latter finding, which is qualitatively consistent with the observed decrease in the dimerization constant for LEN from $\sim 4 \times 10^5$ $M^{-1}$ under physiological conditions[18] to $\sim 2 \times 10^4$ $M^{-1}$ at pH 2,[19] suggests that at acidic pH the key hydrogen-bonding interactions involving residues Q38 and Q89 as well as neighboring water molecules become progressively more disrupted, allowing the protein to occupy higher-energy, partially unfolded states with greater frequency.

It is important to reiterate here that the main assumption underlying the interpretation of $^{15}$N CPMG relaxation dispersion data—namely, that the observed relaxation dispersions report on internal protein backbone dynamics within the LEN dimer—is reasonable and that these dispersions and the significant differences between them at physiological and acidic pH are not simply the result of the monomer−dimer equilibrium process and any associated chemical shift changes. First, as already discussed in detail above, the strong correlations in $^1$H, $^{15}$N, and $^{13}C^{\alpha}$ chemical shifts, which include shifts for a number of residues found near the dimer interface, and effectively identical rotational correlation times obtained from the ps−ns time scale dynamics analysis indicate no significant differences in the structure and oligomeric state of LEN at pH 6.5 and 2.0. In addition, to probe this issue more directly we have recorded a set of $^{15}$N CPMG relaxation dispersion trajectories at 800 MHz $^1$H frequency for a sample of $^{15}$N-LEN at pH 6.5 diluted to 0.8 mM—i.e., having a protein concentration that is lower by more than a factor of 2, and thus an increased fraction of LEN in the monomeric state, relative to samples used to record the relaxation data in Figure 4. The fact that no significant differences are observed for any of the residue-specific relaxation dispersion trajectories between the 0.8 and 1.7 mM LEN samples (Supporting Information Figure S5) confirms that at protein concentrations employed in this study these dispersions can be interpreted exclusively in terms of internal dynamics of the LEN dimer and that any contributions due to the monomer−dimer equilibrium process are negligible.

Under agitation, protein molecules including antibody fragments have been found to adsorb at the air−water interface, resulting in hydrophobic stress, destabilization of native structure to form partially unfolded states, and, ultimately, aggregation.[69,70] At acidic pH, though still largely a properly folded dimer, LEN exists in an aggregation-competent state, where a number of amino acid residues along the dimer interface display significant conformational flexibility that interferes with the maintenance of proper hydrogen-bonding interactions between the individual monomer subunits. Nonetheless, since LEN is incapable of forming amyloid in the absence of agitation,[6,19−22] a ∼10−15% population of the excited-state protein conformers present at pH 2 is alone clearly insufficient to tip the system toward aggregation. The agitation process thus appears to be required to overcome the additional energy barrier for aggregation by generating a higher concentration of misfolded amyloidogenic protein states, possibly with further residues in the vicinity of the three most flexible regions experiencing elevated dynamics on the ms time scale. Moreover, in retrospect, these findings imply that mere agitation of LEN under physiological conditions does not lead to aggregation because the partially unfolded, higher-energy states are accessed for only a small fraction of time, owing to the sufficiently high degree of dimer interface stabilization by the network of hydrogen bonds.

While additional NMR studies, including site-resolved measurements of $^{1}H^{N}$, $^{13}CO$, and $^{13}C^{\alpha}$ relaxation dispersion,[29] are necessary to generate more precise models of the partially unfolded states of LEN through which conversion from the native state to amyloid can occur, the current study clearly identifies the key amino acid residues involved in the earliest stages of protein misfolding and lays the foundation for future investigations along these lines. Interestingly, the light-chain variable domain SMA, which is highly homologous to LEN and associated with development of AL amyloidosis,[17,18] has been found to exhibit, under physiological conditions, many characteristics of LEN at pH ∼2.[19−21,23] This suggests that the main findings of this work, linking the conformational dynamics of a specific set of residues colocalized at the dimer interface to populating higher-energy partially misfolded protein conformers, are relevant for understanding, at the molecular level, the primary driving forces behind amyloid formation for disease-related Ig $V_L$ variants and the effects of site-specific mutations on the aggregation propensities of these proteins.[5,6] Finally, the identification of specific residues and regions involved in the earliest stages of protein unfolding may aid in the rational design of therapeutics that stabilize the tertiary and quaternary structure and prevent aggregation of these immunoglobulin light-chain domains, in analogy to transthyretin,[71] superoxide dismutase,[72] and other amyloidogenic proteins.[2]

## ■ ASSOCIATED CONTENT

**Supporting Information.** Figures S1−S5 showing regions of LEN $^{15}N-^{1}H$ HSQC NMR spectra recorded at different pH values, plots of $^{15}N$ spin relaxation data and $^{15}N$ CPMG relaxation dispersion trajectories, and Tables S1 and S2 containing $^{15}N$ spin relaxation data and results of model-free analysis. This material is available free of charge via the Internet at http://pubs.acs.org.

## ■ AUTHOR INFORMATION

### Corresponding Author

*Phone: (614) 247-4284. Fax: (614) 292-1685. E-mail: jaroniec@chemistry.ohio-state.edu.

### Funding Sources

This work was supported by grants from the American Heart Association (0865410D to C.P.J. and Postdoctoral Fellowship 09POST2220178 to S.M.).

## ■ ACKNOWLEDGMENT

We thank Dr. Fred J. Stevens for the LEN plasmid and Drs. Arthur G. Palmer, Lewis E. Kay, and their group members for access to data analysis software and stimulating discussions.

## ■ ABBREVIATIONS

NMR, nuclear magnetic resonance; CPMG, Carr−Purcell−Meiboom−Gill; AL, light-chain amyloidosis; Ig $V_L$, immunoglobulin light-chain variable domain; CDR, complementarity determining region; aa, amino acid; 2D, two-dimensional; 3D, three-dimensional; HSQC, heteronuclear single quantum coherence; HMQC, heteronuclear multiple quantum coherence; RF, radio frequency; FID, free-induction decay; NOE, nuclear Overhauser enhancement; CSA, chemical shift anisotropy; ps, picosecond; ns, nanosecond; ms, millisecond; rms, root-mean-square.

## ■ REFERENCES

(1) Chiti, F., and Dobson, C. M. (2006) Protein misfolding, functional amyloid, and human disease. *Annu. Rev. Biochem. 75*, 333–366.

(2) Chiti, F., and Dobson, C. M. (2009) Amyloid formation by globular proteins under native conditions. *Nat. Chem. Biol. 5*, 15–22.

(3) Solomon, A., and Weiss, D. T. (1995) Protein and host factors implicated in the pathogenesis of light chain amyloidosis (AL amyloidosis). *Amyloid 2*, 269–279.

(4) Falk, R. H., Comenzo, R. L., and Skinner, M. (1997) The systemic amyloidoses. *N. Engl. J. Med. 337*, 898–909.

(5) Hurle, M. R., Helms, L. R., Li, L., Chan, W., and Wetzel, R. (1994) A role for destabilizing amino acid replacements in light-chain amyloidosis. *Proc. Natl. Acad. Sci. U.S.A. 91*, 5446–5450.

(6) Raffen, R., Dieckman, L. J., Szpunar, M., Wunschl, C., Pokkuluri, P. R., Dave, P., Wilkins Stevens, P., Cai, X., Schiffer, M., and Stevens, F. J. (1999) Physicochemical consequences of amino acid variations that contribute to fibril formation by immunoglobulin light chains. *Protein Sci. 8*, 509–517.

(7) Kim, Y. S., Wall, J. S., Meyer, J., Murphy, C., Randolph, T. W., Manning, M. C., Solomon, A., and Carpenter, J. F. (2000) Thermodynamic modulation of light chain amyloid fibril formation. *J. Biol. Chem. 275*, 1570–1574.

(8) Baden, E. M., Randles, E. G., Aboagye, A. K., Thompson, J. R., and Ramirez-Alvarado, M. (2008) Structural insights into the role of mutations in amyloidogenesis. *J. Biol. Chem. 283*, 30950–30956.

(9) Baden, E. M., Sikkink, L. A., and Ramirez-Alvarado, M. (2009) Light chain amyloidosis: Current findings and future prospects. *Curr. Protein Pept. Sci. 10*, 500–508.

(10) Epp, O., Lattman, E. E., Schiffer, M., Huber, R., and Palm, R. (1975) The molecular structure of a dimer composed of the variable portions of the Bence-Jones protein REI refined at 2.0 Å resolution. *Biochemistry 14*, 4943–4952.

(11) Huang, D. B., Chang, C. H., Ainsworth, C., Brunger, A. T., Eulitz, M., Solomon, A., Stevens, F. J., and Schiffer, M. (1994) Comparison of two homologous proteins: Structural origin of altered domain interactions in immunoglobulin light-chain dimers. *Biochemistry 33*, 14848–14857.

(12) Schormann, N., Murrell, J. R., Liepnieks, J. J., and Benson, M. D. (1995) Tertiary structure of an amyloid immunoglobulin light chain protein: A proposed model for amyloid fibril formation. *Proc. Natl. Acad. Sci. U.S.A. 92*, 9490–9494.

(13) Bourne, P. C., Ramsland, P. A., Shan, L., Fan, Z. C., DeWitt, C. R., Shultz, B. B., Terzyan, S. S., Moomaw, C. R., Slaughter, C. A., Guddat, L. W., and Edmundson, A. B. (2002) Three-dimensional structure of an

immunoglobulin light-chain dimer with amyloidogenic properties. *Acta Crystallogr., Sect. D: Biol. Crystallogr. 58*, 815–823.

(14) Wall, J. S., Gupta, V., Wilkerson, M., Schell, M., Loris, R., Adams, P., Solomon, A., Stevens, F., and Dealwis, C. (2004) Structural basis of light chain amyloidogenicity: comparison of the thermodynamic properties, fibrillogenic potential and tertiary structural features of four Vλ6 proteins. *J. Mol. Recognit. 17*, 323–331.

(15) Baden, E. M., Owen, B. A., Peterson, F. C., Volkman, B. F., Ramirez-Alvarado, M., and Thompson, J. R. (2008) Altered dimer interface decreases stability in an amyloidogenic protein. *J. Biol. Chem. 283*, 15853–15860.

(16) Eichner, T., Kalverda, A. P., Thompson, G. S., Homans, S. W., and Radford, S. E. (2011) Conformational conversion during amyloid formation at atomic resolution. *Mol. Cell 41*, 161–172.

(17) Solomon, A. (1985) Light chains of human immunoglobulins. *Methods Enzymol. 116*, 101–121.

(18) Wilkins Stevens, P., Raffen, R., Hanson, D. K., Deng, Y. L., Berrios-Hammond, M., Westholm, F. A., Murphy, C., Eulitz, M., Wetzel, R., Solomon, A., Schiffer, M., and Stevens, F. J. (1995) Recombinant immunoglobulin variable domains generated from synthetic genes provide a system for in vitro characterization of light-chain amyloid proteins. *Protein Sci. 4*, 421–432.

(19) Souillac, P. O., Uversky, V. N., Millett, I. S., Khurana, R., Doniach, S., and Fink, A. L. (2002) Elucidation of the molecular mechanism during the early events in immunoglobulin light chain amyloid fibrillation: Evidence for an off-pathway oligomer at acidic pH. *J. Biol. Chem. 277*, 12666–12679.

(20) Souillac, P. O., Uversky, V. N., and Fink, A. L. (2003) Structural transformations of oligomeric intermediates in the fibrillation of the immunoglobulin light chain LEN. *Biochemistry 42*, 8094–8104.

(21) Khurana, R., Souillac, P. O., Coats, A. C., Minert, L., Ionescu-Zanetti, C., Carter, S. A., Solomon, A., and Fink, A. L. (2003) A model for amyloid fibril formation in immunoglobulin light chains based on comparison of amyloidogenic and benign proteins and specific antibody binding. *Amyloid 10*, 97–109.

(22) Souillac, P. O., Uversky, V. N., Millett, I. S., Khurana, R., Doniach, S., and Fink, A. L. (2002) Effect of association state and conformational stability on the kinetics of immunoglobulin light chain amyloid fibril formation at physiological pH. *J. Biol. Chem. 277*, 12657–12665.

(23) Khurana, R., Gillespie, J. R., Talapatra, A., Minert, L. J., Ionescu-Zanetti, C., Millett, I., and Fink, A. L. (2001) Partially folded intermediates as critical precursors of light chain amyloid fibrils and amorphous aggregates. *Biochemistry 40*, 3525–3535.

(24) Jarymowycz, V. A., and Stone, M. J. (2006) Fast time scale dynamics of protein backbones: NMR relaxation methods, applications, and functional consequences. *Chem. Rev. 106*, 1624–1671.

(25) Palmer, A. G. (2004) NMR characterization of the dynamics of biomacromolecules. *Chem. Rev. 104*, 3623–3640.

(26) Cavanagh, J., Fairbrother, W. J., Palmer, A. G., Rance, M., and Skelton, N. J. (2007) *Protein NMR Spectroscopy: Principles and Practice*, Elsevier Academic Press, San Diego, CA.

(27) Ishima, R., and Torchia, D. A. (2000) Protein dynamics from NMR. *Nat. Struct. Biol. 7*, 740–743.

(28) Henzler-Wildman, K., and Kern, D. (2007) Dynamic personalities of proteins. *Nature 450*, 964–972.

(29) Baldwin, A. J., and Kay, L. E. (2009) NMR spectroscopy brings invisible protein states into focus. *Nat. Chem. Biol. 5*, 808–814.

(30) Liu, K., Cho, H. S., Lashuel, H. A., Kelly, J. W., and Wemmer, D. E. (2000) A glimpse of a possible amyloidogenic intermediate of transthyretin. *Nat. Struct. Biol. 7*, 754–757.

(31) Liu, K., Kelly, J. W., and Wemmer, D. E. (2002) Native state hydrogen exchange study of suppressor and pathogenic variants of transthyretin. *J. Mol. Biol. 320*, 821–832.

(32) Dumoulin, M., Canet, D., Last, A. M., Pardon, E., Archer, D. B., Muyldermans, S., Wyns, L., Matagne, A., Robinson, C. V., Redfield, C., and Dobson, C. M. (2005) Reduced global cooperativity is a common feature underlying the amyloidogenicity of pathogenic lysozyme mutations. *J. Mol. Biol. 346*, 773–788.

(33) Carulla, N., Zhou, M., Giralt, E., Robinson, C. V., and Dobson, C. M. (2010) Structure and intermolecular dynamics of aggregates populated during amyloid fibril formation studied by hydrogen/deuterium exchange. *Acc. Chem. Res. 43*, 1072–1079.

(34) Hoshino, M., Katou, H., Hagihara, Y., Hasegawa, K., Naiki, H., and Goto, Y. (2002) Mapping the core of the $\beta_2$-microglobulin amyloid fibril by H/D exchange. *Nat. Struct. Biol. 9*, 332–336.

(35) Hoshino, M., Katou, H., Yamaguchi, K., and Goto, Y. (2007) Dimethylsulfoxide-quenched hydrogen/deuterium exchange method to study amyloid fibril structure. *Biochim. Biophys. Acta 1768*, 1886–1899.

(36) Serag, A. A., Altenbach, C., Gingery, M., Hubbell, W. L., and Yeates, T. O. (2002) Arrangement of subunits and ordering of $\beta$-strands in an amyloid sheet. *Nat. Struct. Biol. 9*, 734–739.

(37) Margittai, M., and Langen, R. (2008) Fibrils with parallel in-register structure constitute a major class of amyloid fibrils: molecular insights from electron paramagnetic resonance spectroscopy. *Q. Rev. Biophys. 41*, 265–297.

(38) Tycko, R. (2006) Molecular structure of amyloid fibrils: insights from solid-state NMR. *Q. Rev. Biophys. 39*, 1–55.

(39) Heise, H. (2008) Solid-state NMR spectroscopy of amyloid proteins. *ChemBioChem 9*, 179–189.

(40) Mukherjee, S., Pondaven, S. P., Höfer, N., and Jaroniec, C. P. (2009) Backbone and sidechain $^1$H, $^{13}$C and $^{15}$N resonance assignments of LEN, a human immunoglobulin κIV light-chain variable domain. *Biomol. NMR Assign. 3*, 255–259.

(41) Cavanagh, J., Palmer, A. G., Wright, P. E., and Rance, M. (1991) Sensitivity improvement in proton detected 2-dimensional heteronuclear relay spectroscopy. *J. Magn. Reson. 91*, 429–436.

(42) Kay, L. E., Keifer, P., and Saarinen, T. (1992) Pure absorption gradient enhanced heteronuclear single quantum correlation spectroscopy with improved sensitivity. *J. Am. Chem. Soc. 114*, 10663–10665.

(43) Wang, A. C., and Bax, A. (1993) Minimizing the effects of radio-frequency heating in multidimensional NMR experiments. *J. Biomol. NMR 3*, 715–720.

(44) Farrow, N. A., Muhandiram, R., Singer, A. U., Pascal, S. M., Kay, C. M., Gish, G., Shoelson, S. E., Pawson, T., Forman-Kay, J. D., and Kay, L. E. (1994) Backbone dynamics of a free and a phosphopeptide-complexed Src homology 2 domain studied by $^{15}$N NMR relaxation. *Biochemistry 33*, 5984–6003.

(45) Tjandra, N., Szabo, A., and Bax, A. (1996) Protein backbone dynamics and N-15 chemical shift anisotropy from quantitative measurement of relaxation interference effects. *J. Am. Chem. Soc. 118*, 6986–6991.

(46) Kroenke, C. D., Loria, J. P., Lee, L. K., Rance, M., and Palmer, A. G. (1998) Longitudinal and transverse $^1$H-$^{15}$N dipolar $^{15}$N chemical shift anisotropy relaxation interference: Unambiguous determination of rotational diffusion tensors and chemical exchange effects in biological macromolecules. *J. Am. Chem. Soc. 120*, 7905–7915.

(47) Palmer, A. G., Kroenke, C. D., and Loria, J. P. (2001) NMR methods for quantifying microsecond-to-millisecond motions in biological macromolecules. *Methods Enzymol. 339*, 204–238.

(48) Wang, C. Y., and Palmer, A. G. (2003) Solution NMR methods for quantitative identification of chemical exchange in $^{15}$N-labeled proteins. *Magn. Reson. Chem. 41*, 866–876.

(49) Hansen, D. F., Vallurupalli, P., and Kay, L. E. (2008) An improved $^{15}$N relaxation dispersion experiment for the measurement of millisecond time-scale dynamics in proteins. *J. Phys. Chem. B 112*, 5898–5904.

(50) Tollinger, M., Skrynnikov, N. R., Mulder, F. A. A., Forman-Kay, J. D., and Kay, L. E. (2001) Slow dynamics in folded and unfolded states of an SH3 domain. *J. Am. Chem. Soc. 123*, 11341–11352.

(51) Korzhnev, D. M., Salvatella, X., Vendruscolo, M., Di Nardo, A. A., Davidson, A. R., Dobson, C. M., and Kay, L. E. (2004) Low-populated folding intermediates of Fyn SH3 characterized by relaxation dispersion NMR. *Nature 430*, 586–590.

(52) Delaglio, F., Grzesiek, S., Vuister, G. W., Zhu, G., Pfeifer, J., and Bax, A. (1995) NMRPipe: a multidimensional spectral processing system based on UNIX pipes. *J. Biomol. NMR 6*, 277–293.

(53) Kay, L. E., Torchia, D. A., and Bax, A. (1989) Backbone dynamics of proteins as studied by $^{15}$N inverse detected heteronuclear

NMR spectroscopy: Application to staphylococcal nuclease. *Biochemistry 28*, 8972–8979.

(54) http://www.palmer.hs.columbia.edu/software.html.

(55) Tjandra, N., Feller, S. E., Pastor, R. W., and Bax, A. (1995) Rotational diffusion anisotropy of human ubiquitin from $^{15}$N NMR relaxation. *J. Am. Chem. Soc. 117*, 12562–12566.

(56) Huang, D. B., Chang, C. H., Ainsworth, C., Johnson, G., Solomon, A., Stevens, F. J., and Schiffer, M. (1997) Variable domain structure of κIV human light chain Len: High homology to the murine light chain McPC603. *Mol. Immunol. 34*, 1291–1301.

(57) Lipari, G., and Szabo, A. (1982) Model-free approach to the interpretation of nuclear magnetic resonance relaxation in macromolecules. 1. theory and range of validity. *J. Am. Chem. Soc. 104*, 4546–4559.

(58) Lipari, G., and Szabo, A. (1982) Model-free approach to the interpretation of nuclear magnetic resonance relaxation in macromolecules. 2. Analysis of experimental results. *J. Am. Chem. Soc. 104*, 4559–4570.

(59) Cole, R., and Loria, J. P. (2003) FAST-Modelfree: A program for rapid automated analysis of solution NMR spin-relaxation data. *J. Biomol. NMR 26*, 203–213.

(60) Mandel, A. M., Akke, M., and Palmer, A. G. (1995) Backbone dynamics of Escherichia coli ribonuclease HI: Correlations with structure and function in an active enzyme. *J. Mol. Biol. 246*, 144–163.

(61) Butterwick, J. A., Loria, J. P., Astrof, N. S., Kroenke, C. D., Cole, R., Rance, M., and Palmer, A. G. (2004) Multiple time scale backbone dynamics of homologous thermophilic and mesophilic ribonuclease HI enzymes. *J. Mol. Biol. 339*, 855–871.

(62) Carver, J. P., and Richards, R. E. (1972) General two-site solution for the chemical exchange produced dependence of T2 upon the Carr-Purcell pulse separation. *J. Magn. Reson. 6*, 89–105.

(63) http://abragam.med.utoronto.ca/software.html.

(64) Skrynnikov, N. R., Dahlquist, F. W., and Kay, L. E. (2002) Reconstructing NMR spectra of "invisible" excited protein states using HSQC and HMQC experiments. *J. Am. Chem. Soc. 124*, 12352–12360.

(65) Spera, S., and Bax, A. (1991) Empirical correlation between protein backbone conformation and Cα and Cβ $^{13}$C nuclear magnetic resonance chemical shifts. *J. Am. Chem. Soc. 113*, 5490–5492.

(66) Clore, G. M., Szabo, A., Bax, A., Kay, L. E., Driscoll, P. C., and Gronenborn, A. M. (1990) Deviations from the simple two-parameter model-free approach to the interpretation of nitrogen-15 nuclear magnetic relaxation of proteins. *J. Am. Chem. Soc. 112*, 4989–4991.

(67) http://www.bmrb.wisc.edu.

(68) Pokkuluri, P. R., Huang, D. B., Raffen, R., Cai, X., Johnson, G., Stevens, P. W., Stevens, F. J., and Schiffer, M. (1998) A domain flip as a result of a single amino-acid substitution. *Structure 6*, 1067–1073.

(69) Sluzky, V., Tamada, J. A., Klibanov, A. M., and Langer, R. (1991) Kinetics of insulin aggregation in aqueous solutions upon agitation in the presence of hydrophobic surfaces. *Proc. Natl. Acad. Sci. U.S.A. 88*, 9377–9381.

(70) Mahler, H. C., Muller, R., Friess, W., Delille, A., and Matheus, S. (2005) Induction and analysis of aggregates in a liquid IgG1-antibody formulation. *Eur. J. Pharm. Biopharm. 59*, 407–417.

(71) Johnson, S. M., Wiseman, R. L., Sekijima, Y., Green, N. S., Adamski-Werner, S. L., and Kelly, J. W. (2005) Native state kinetic stabilization as a strategy to ameliorate protein misfolding diseases: a focus on the transthyretin amyloidoses. *Acc. Chem. Res. 38*, 911–921.

(72) Ray, S. S., Nowak, R. J., Brown, R. H., and Lansbury, P. T. (2005) Small-molecule-mediated stabilization of familial amyotrophic lateral sclerosis-linked superoxide dismutase mutants against unfolding and aggregation. *Proc. Natl. Acad. Sci. U.S.A. 102*, 3639–3644.